The Impact of Aggregation on the Photophysics of Spiro-bridged Heterotriangulenes

Marcel Krug, Maximilian Wagner, Tobias A Schaub, Wen-Shan Zhang, Christoph M Schüsslbauer, Johannes D R Ascherl, Peter W Münich, Rasmus R Schröder, Franziska Gröhn, Pavlo O Dral, et al.

A Journal of the Gesellschaft Deutscher Chemiker

Angewandte International Edition GDCh Chemie

www.angewandte.org

Accepted Article

Title: The Impact of Aggregation on the Photophysics of Spiro-bridged Heterotriangulenes

Authors: Milan Kivala, Marcel Krug, Maximilian Wagner, Tobias A. Schaub, Wen-Shan Zhang, Christoph M. Schüßlbauer, Johannes D. R. Ascherl, Peter W. Münich, Rasmus R. Schröder, Franziska Gröhn, Pavlo O. Dral, Mario Barbatti, and Dirk M. Guldi

To be cited as: *Angew. Chem. Int. Ed.* 10.1002/anie.202003504

Link to VoR: https://doi.org/10.1002/anie.202003504

WILEY-VCH

10.1002/anie.202003504

WILEY-VCH

RESEARCH ARTICLE

The Impact of Aggregation on the Photophysics of Spiro-bridged Heterotriangulenes

Marcel Krug,[a] Maximilian Wagner,[a] Tobias A. Schaub,[b] Wen-Shan Zhang,[c] Christoph M. Schüßlbauer,[a] Johannes D. R. Ascherl,[b,c] Peter W. Münich,[a] Rasmus R. Schröder,[c] Franziska Gröhn,[a] Pavlo O. Dral,[d] Mario Barbatti,[e] Dirk M. Guldi,[a]* Milan Kivala[b,c]*

[a] M. Krug, M. Wagner, C. M. Schüßlbauer, Dr. P. W. Münich, Prof. Dr. F. Gröhn, Prof. Dr. D. M. Guldi
Department of Chemistry and Pharmacy, Interdisciplinary Center for Molecular Materials (ICMM)
Friedrich-Alexander-Universität Erlangen-Nürnberg
Egerlandstrasse 3, 91058 Erlangen, Germany
E-mail: dirk.guldi@fau.de

[b] Dr. T. A. Schaub, J. D. R. Ascherl, Prof. Dr. M. Kivala
Organisch-Chemisches Institut
Ruprecht-Karls-Universität Heidelberg
Im Neuenheimer Feld 270, 69120 Heidelberg, Germany
E-mail: milan.kivala@oci.uni-heidelberg.de

[c] Dr. W.-S. Zhang, J. D. R. Ascherl, Prof. Dr. R. R. Schröder, Prof. Dr. M. Kivala
Centre for Advanced Materials
Ruprecht-Karls-Universität Heidelberg
Im Neuenheimer Feld 225, 69120 Heidelberg, Germany

[d] Prof. Dr. P. O. Dral
State Key Laboratory of Physical Chemistry of Solid Surfaces, Fujian Provincial Key Laboratory of Theoretical and Computational Chemistry, Department of Chemistry, and College of Chemistry and Chemical Engineering
Xiamen University
Xiamen 361005, China

[e] Prof. Dr. M. Barbatti
Aix Marseille University, CNRS, ICR, Marseille, France

Supporting information for this article is given via a link at the end of the document.

Abstract: We report on the impact of the central heteroatom on structural, electronic, and spectroscopic properties in a series of spirofluorene-bridged heterotriangulenes and provide a detailed study on their aggregates. The in-depth analysis of their molecular structure by NMR spectroscopy and X-ray crystallography was further complemented by density functional theory calculations. With the aid of extensive photophysical analysis the complex fluorescence spectra were deconvoluted showing contributions from the peripheral fluorenes and the heteroaromatic cores. Beyond the molecular scale, we examined the aggregation behavior of these heterotriangulenes in THF/H_2O mixtures and analyzed the aggregates by static and dynamic light scattering. The excited-state interactions within the aggregates were found to be similar to those found in the solid state. A plethora of morphologies and superstructures were observed by scanning electron microscopy of drop-casted dispersions.

Introduction

The fabrication of functional organic materials starting from small molecular building blocks is a challenging, yet appealing task. However, the prediction and guided design of molecular materials and their functionalities is far from being fully understood.[1,2]
In this context, taking molecular aggregates as the simplest blueprint enables understanding the corresponding changes, which are linked to the formation of close intermolecular contacts that govern the self-assembly.[3–5] Of particular avail is the control over aggregation as a dynamic process by external influences, namely temperature,[6] solvent effects,[7,8] concentration,[9,10] or solubility,[11] and the tailored design of the molecular building blocks.[12–15]

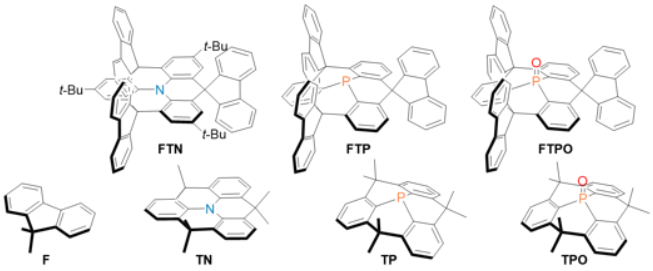

Figure 1: Chemical structures of 9,9-dimethylfluorene (**F**), the heterotriangulenes (**TN**, **TP**, and **TPO**), and the spiro-bridged heterotriangulenes (**FTN**, **FTP**, **FTPO**).

The aforementioned interactions between individual molecules within the aggregates can alter their electronic structure and therefore also their spectroscopic properties with respect to the isolated species. In the ground state, the relative orientation of the building blocks manifests in hypsochromic or bathochromic shifts in the absorption spectrum and reveals the presence of H- or J-aggregates.[16–20] In the excited state, photophysical phenomena are even more complex. At proximity, the molecular building blocks favor the formation of either excimers or exciplexes with emissive features significantly different from those of the individual components.[7,21,22] Strongly distance-dependent deactivation processes such as excited-state energy,[20,21,23,24] charge,[25] or electron transfer[23] are facilitated between molecules in confined space. The lack of molecular rotations

10.1002/anie.202003504

leads to aggregation induced / enhanced emission, which strongly favors radiative deactivations.[24,26–29]

Herein, we present a systematic study of the properties of a series of related heteroatom-containing polycyclic aromatic hydrocarbons – namely spirofluorene-bridged triarylamine[30], -phosphine, and -phosphine oxide[31] – in the transition from molecular species to large aggregates (Figure 1).

Initially, their structural aspects were disclosed by X-ray crystallography and DFT calculations aided to rationalize the observed optical features of the molecular entities and their intermolecular interactions in the bulk. In the focus of this study, the degree of aggregation for these compounds was varied and the concomitant photophysical and morphological changes were probed by UV/vis absorption, emission spectroscopy, dynamic light scattering (DLS), and scanning electron microscopy (SEM). This systematic approach enabled us to gather a sound understanding of the impact of aggregation on the photophysical properties of this intriguing class of compounds.

Results and Discussion

While the syntheses of compounds **FTN**[30] and **FTPO**[31] have recently been reported by us, spiro-bridged triarylphosphine **FTP** had yet to be prepared (Figure 1). We commenced our synthetic efforts by subjecting **FTPO** to various conventional reducing agents, such as $HSiCl_3$, $LiAlH_4$ as well as more complex systems such as *Imamoto's* MeOTf/$LiAlH_4$[32] and the Ti(*i*-OPr)$_4$/$HSi(OEt)_3$ pair reported by *Lawrence* and coworkers.[33] All of these methods failed to reduce **FTPO**, which we ascribed to the challenging nature of this conversion most likely owing to the steric bulk around the central phosphoryl unit. We were pleased, though, to find that *Lemaire's* optimized reducing system consisting of a mixture of $PhSiH_3$ and $HSiCl_3$ was capable to perform the desired conversion to **FTP** in excellent yields (Figure 2a, for synthetic details, see the Supporting Information (SI), section 3).[34] **FTP** was isolated as a benchtop stable colorless microcrystalline powder, which slowly oxidized back to **FTPO** in solution under ambient conditions over a time period of several days.

With the complete series of spiro-bridged scaffolds in hands, we first turned our attention to their structural characterization. On the timescale of NMR spectroscopy, **FTN** displays an overall D_{3h} symmetry with five distinct peaks in the aromatic region (Figure 2b).[30] In contrast, inward bending of the orthogonal fluorenyl units to the center of the rigidified scaffolds of **FTP** and **FTPO** – *vide infra* – results in lowering of the symmetry and a splitting of the ^{1}H resonances of the fluorenyl moieties. A weak overall downfield shift of the ^{1}H signals is observed when going from **FTN** to **FTP** and **FTPO** (Figure 2c, for complete assignment of the ^{1}H signals, see the SI). This trend is rationalized by considering the balance between mesomeric and inductive effects of the heteroatoms, which is similar to the known trends in NPh_2, PPh_2, and $O{=}PPh_2$ groups.[35] Nitrogen has an overall electron-donating character, that is, +M effect larger than −I effect, phosphorus an overall electron-withdrawing character, that is, weak −I effect and negligible mesomeric effect, and the P=O group has an electron-withdrawing character due to a strong –M effect and pronounced −I effect.[35] Such a trend in a series of our spiro-compounds is corroborated by calculated Mulliken charges on heteroatoms: +0.224 *e* on N in **FTN**, −0.257 *e* on P in **FTP**, and +0.415 *e* on P and −0.642 *e* on O in **FTPO**. Accordingly, in ^{31}P NMR (162.0 MHz, $C_2D_2Cl_4$) experiments we find a pronounced upfield shift for **FTP** (δ −71.5 ppm, compared to **FTPO** −21.0 ppm). The observed electronic parameters are viewed within the concept of negative hyperconjugation, effectively creating a strongly electron-withdrawing phosphorus center in **FTPO**; an effect which is absent in **FTP**.[36–38]

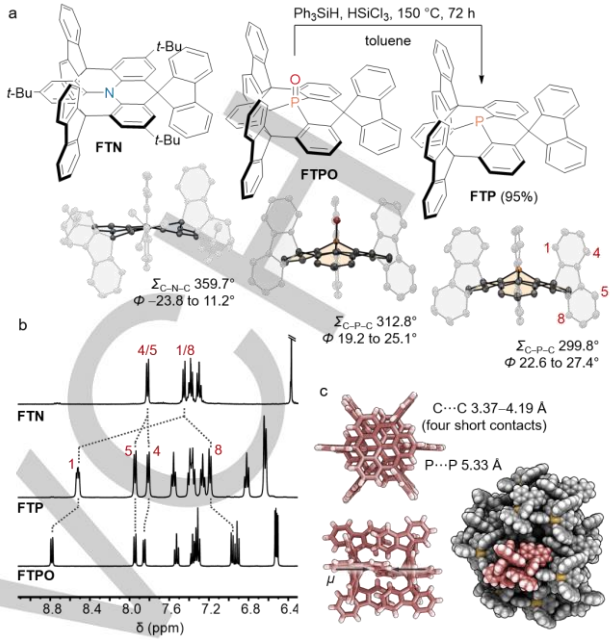

Figure 2: a) Molecular X-ray structures of **FTN**, **FTPO**, and **FTP**; **FTP** was synthesized from **FTPO** by silane-mediated reduction; b) ^{1}H NMR spectrum (400.1 MHz, CD_2Cl_2) and assignment of selected signals; c) Illustration of an **FTP** aggregate, generated from the X-ray structure (molecular shell of 7 Å diameter) and cut out of the interdigitating dimers formed in the crystalline state.

The molecular structure of **FTP** was unambiguously assigned by X-ray crystallography and, with the recent reports for **FTN**[30] and **FTPO**,[31] provide a complete data set. Single crystals of **FTP** were grown by slow liquid-liquid diffusion of deaerated *n*-hexane into a solution of **FTP** in deaerated benzene at room temperature. Upon removal of the phosphoryl oxygen in **FTP** the overall molecular structure — a bowl shaped core with a tripod-like fluorene-based periphery — is retained. Hypothetical planar **FTP** corresponds to the transition state of the bowl inversion with a *Gibbs* activation energy $\Delta G^{\ddagger}_{298}$ of 46.6 kcal mol^{-1} calculated using DFT (ωB97X-D functional,[39] see the SI, section 7.3 for details) and is therefore highly unfavorable. Reduction of the P(V) to a P(III) center leads to significant changes in its geometry. The pyramidalization in **FTP** ($\Sigma_{C–P–C}$ 299.8°) is increased compared to **FTPO** ($\Sigma_{C–P–C}$ 312.8°), which is accompanied by a deeper bowl of **FTP** (1.74 Å, compared to 1.50 Å in **FTPO**).[30,31] The average P–C_{av} bonds in **FTP** (1.792(2) Å) are elongated with respect to **FTPO** (1.762(2) Å). These geometrical features of **FTP** and **FTPO** are essentially the same in vacuum (see analysis of geometries optimized at the ωB97X-D/def2-TZVP[40] level of theory in the SI, section 7.2). As a response to the increased steric constraint of the triarylphosphine core the peripheral fluorenyls are bent inwards, which results in larger distortion angles of the fluorenyls in **FTP** (Φ 22.6–27.4°) than in **FTPO** (Φ 19.2.6–25.1°, for definition of Φ and more details on the core geometry, see the SI, section 4).

In marked contrast to the rigid scaffolds of the studied organophosphorus compounds, **FTN**[30] has been reported to display a rather flexible carbon framework, which allows for considerable deformation of the fluorenyls and the planarized triarylamine core. The solid-state arrangement is largely dictated by C(sp^2)–H···π and π···π interactions for all compounds in this series by virtue of their fluorenyl flanks (Figure 2c, for detailed formation of the supramolecular arrangement, see refs. [30] and [31] as well as the SI, section 4). In addition, C(sp^3)–H···π interactions have been reported for **FTN**, while the electronegative phosphoryl oxygen in **FTPO** was previously demonstrated to act as electron-pair-donor in C(sp^2)–H···O and halogen bond interactions.[31,41]

We were surprised to find **FTP** as interdigitating dimers with opposing molecular dipoles in the crystalline state despite a rather significant dipole moment of 1.21 Debye predicted at ωB97X-D/def2-TZVP. To shine light on the specific intermolecular interactions that dictate this arrangement, DFT calculations were performed for both configurations, namely parallel and antiparallel molecular dipoles, at the B3LYP[42,43]/def2-SVP[40] level of theory with and without dispersion corrections (Figure 3). Since the fluorene moieties are bent towards the tip of the triangulene bowl, they are more closely packed in the **FTP** dimer configuration with antiparallel molecular dipoles than in the configuration with parallel dipole moments. This proximity leads to much stronger dispersion interactions between the **FTP** monomers in the configuration with antiparallel dipole moments. The calculations also show that dispersion interaction plays a crucial role for the bonding strength between two monomers similar to observations for sterically crowded labile molecules (for additional details see the SI, section 7.4).[44] When no dispersion corrections are included, optimization of the dimers leads to structures, where the two monomers are much further apart than in the crystal or in structures optimized with dispersion corrections. In addition, without dispersion corrections, both dimers are predicted to be thermodynamically unfavorable in vacuum.

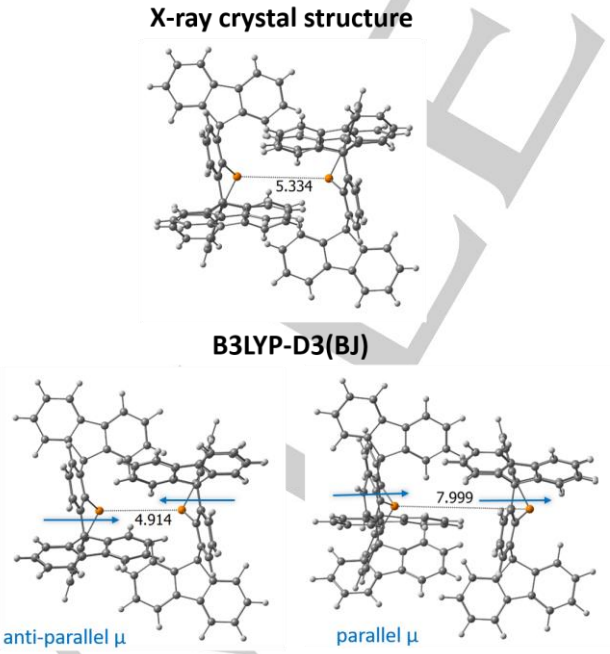

Figure 3: Geometries of **FTP** dimer configurations with anti-parallel and parallel dipole moments from crystal structure and from structures optimized at B3LYP/def2-SVP with dispersion interactions. Distance between two phosphorus atoms is shown in Å. Blue arrows indicate the direction of the molecular dipole moments

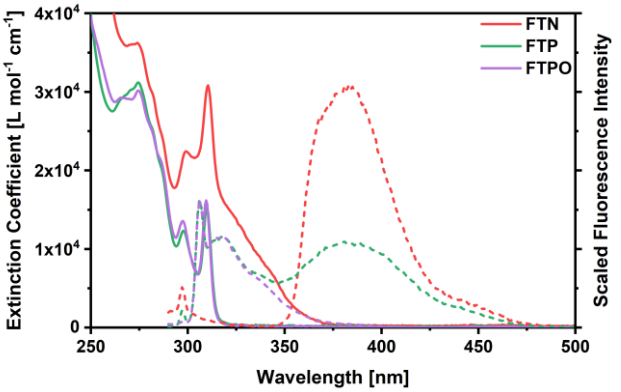

Figure 4: Steady-state absorption (solid lines) and fluorescence spectra (dashed lines) of **FTN**, **FTP**, and **FTPO** in THF at room temperature. λ_{Ex} = 275 nm.

We started the spectroscopic characterization of our spiro-bridged triangulenes (**FTN**, **FTP**, and **FTPO**) by exploration of their electronic ground state properties along with the respective reference compounds (**F**, **TN**, **TP**, and **TPO**)[45,46] by means of steady-state absorption spectroscopy in THF (Figure 4, Figure S11, Table S1). In the absorption spectrum of **FTN**, the electronic transitions are mainly localized on the fluorenes and *N*-heterotriangulenes as follows from the analysis of time-dependent (TD)DFT calculations (at ωB97X-D/def2-TZVP, see the SI, section 7.5). The absorption originating from the three fluorenes appears at 299 and 310 nm ($\varepsilon = 3.08 \times 10^5$ L mol^{-1} cm^{-1}) and overlap with the broad absorption of the *N*-triangulene core, whose red-wavelength flank reaches up to 370 nm.

The analysis of the calculated one-electron transition density matrix (1TDM)[47] between the excited and the ground states also shows that the low-energy transitions are mainly localized on the *N*-triangulene core with a rather significant charge transfer (about 0.4 *e*) to the fluorene moieties. In contrast, the charge transfer character of transitions originating from the fluorenes is very small (about 0.1 *e*; see the SI, section 7.5.5). The lowest energy band in the absorption spectra of **FTP** and **FTPO** originates from the excitations of three fluorenes as follows from theoretical analysis (see the SI, section 7.5.6 and 7.5.7), but is red-shifted with maxima around 310 nm ($\varepsilon = 1.62 \times 10^5$ L mol^{-1} cm^{-1} and $\varepsilon = 1.51 \times 10^5$ L mol^{-1} cm^{-1}, respectively). The second-lowest energy band in **FTP** and **FTPO** at 298 nm is composed of excitations from both fluorene and heterotriangulene core, according to the analysis of TDDFT spectra. We ascribe the red-shifts in the F-centered absorption features to the increased conjugation in the spiro-linked systems originating from the spiro-conjugation.[48–50] In turn, the mismatch between the extinction coefficients of the spiro-compounds and the sum of the extinction coefficients of their respective references is due to electronic interactions already in the ground state.

In our steady-state fluorescence assays (Figures 4 and S11), we focused on the excited-state properties. Photoexcitation of **FTN** generates weak fluorescence with a maximum at 383 nm, but no noteworthy signals are found in the high-energy range between 300-350 nm, where fluorene-based fluorescence is expected. TDDFT calculations confirm that emission originates almost

10.1002/anie.202003504

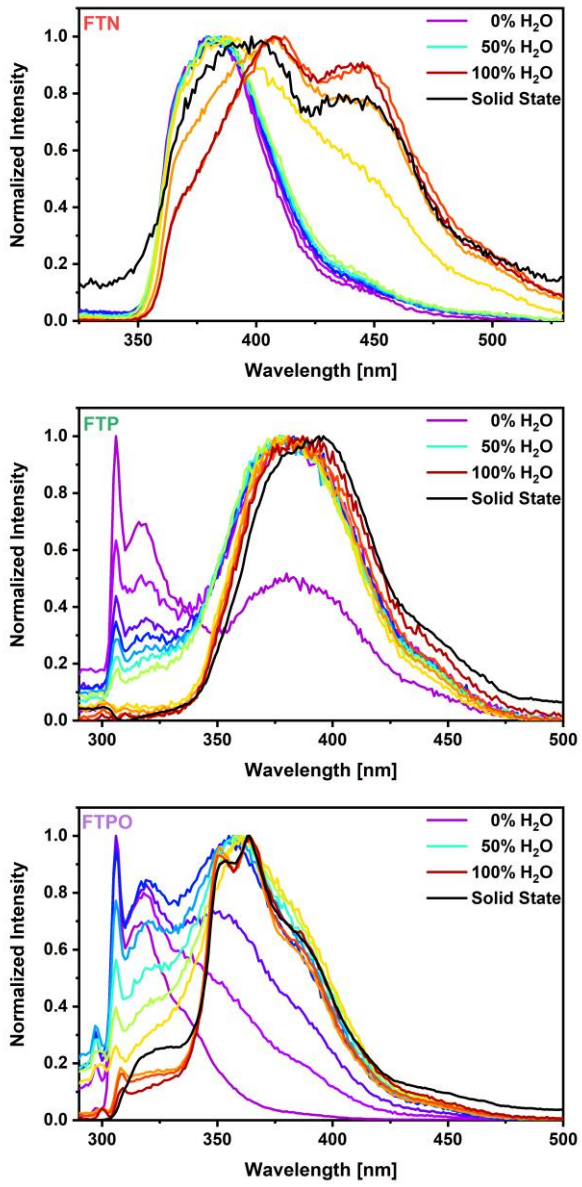

Figure 5: Steady state fluorescence spectra of **FTN** (λ_{Ex} = 275 nm), **FTP** (λ_{Ex} = 260 nm), and **FTPO** (λ_{Ex} = 275 nm) in THF/H_2O mixtures (2 × 10^{-6} M) at room temperature.

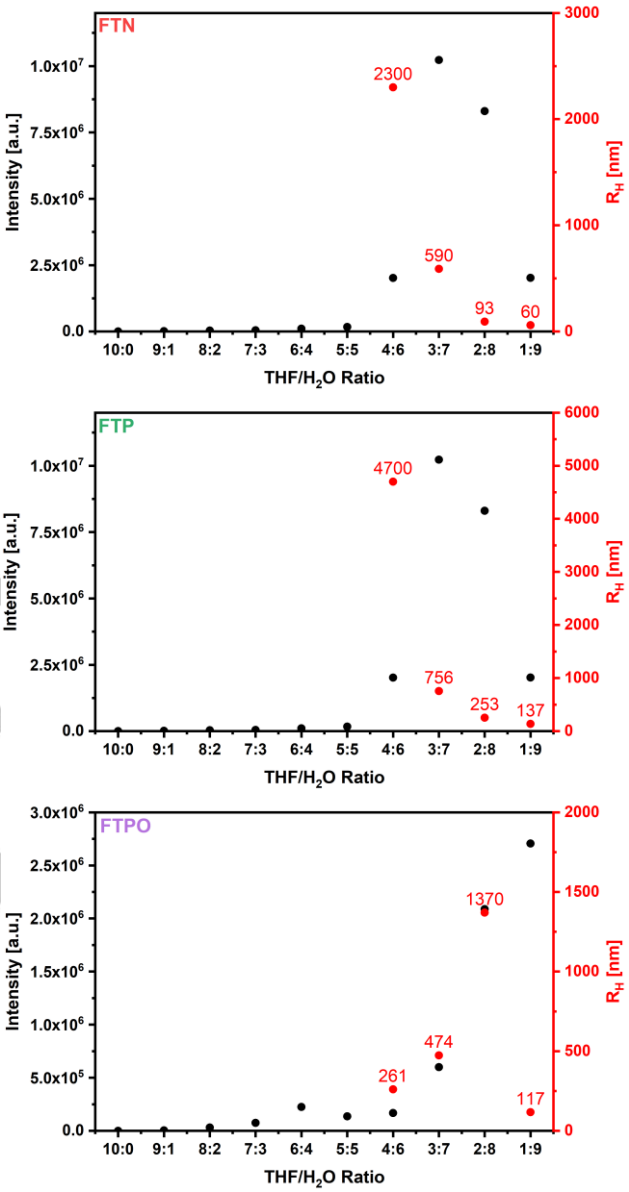

Figure 6: Scattering intensities (black dots) and hydrodynamic radii (red dots) of the spiro-heterotriangulenes in THF/H_2O mixtures (2 × 10^{-6} M).

exclusively from the *N*-triangulene core (SI, Section 7.7). In contrast, **FTP** and **FTPO** exhibit substantial fluorescence in the high-energy fluorene regime with maxima at 306 and 316 nm. This emission stems from a single fluorene according to the analysis of TDDFT calculations. An additional broad band, which peaks around 382 nm, is only noted in the spectrum of **FTP**. Theoretical calculations show that this additional band originates from fluorescence of the *P*-heterotriangulene core.

Aggregation of fluorene and its derivatives is well studied in the literature[21,51–53] and is typically triggered by adding an anti-solvent, such as water. Henceforth, we probed the fluorescent properties of our spiro-heterotriangulenes in THF/H_2O mixtures with increasing water content (Figure 5). The spectrum of **FTN** is barely affected by the presence of water up to 60 vol%. At 70 vol% water, however, a shoulder appears at 450 nm, which further intensifies at even higher water concentrations. At the highest water content, the maxima in the fluorescence spectra are found at 407 and 445 nm. Notably, the original 383 nm feature, which was registered in the absence of any water, is completely absent. **FTP** seems to be even more sensitive to the presence of the anti-solvent water. Within the range of 10 to 60 vol%, the local fluorene-centered fluorescence at 306 and 316 nm declines steadily. With 70 vol% H_2O and beyond, the 382 nm band remains the only feature in the fluorescence spectrum of **FTP**. Likewise, the presence of water induces a decrease of the local fluorene-centered fluorescence in the spectrum of **FTPO**. At the same time, a shoulder emerges in the range of the low-energy flank. The latter transforms into the most prominent feature of the spectrum at water contents between 40 to 70 vol%. At 80 vol% and higher, the fluorescence spectra exhibit band maxima at 351 and 364 nm with a shoulder around 390 nm.

With the help of these experiments, we demonstrated that the emissive properties of our spiro-heterotriangulenes are tunable by the addition of water as the anti-solvent. Two effects should be considered in the following: on the one hand, the increase of the dielectric constant of the solvent continuum and, on the other

10.1002/anie.202003504

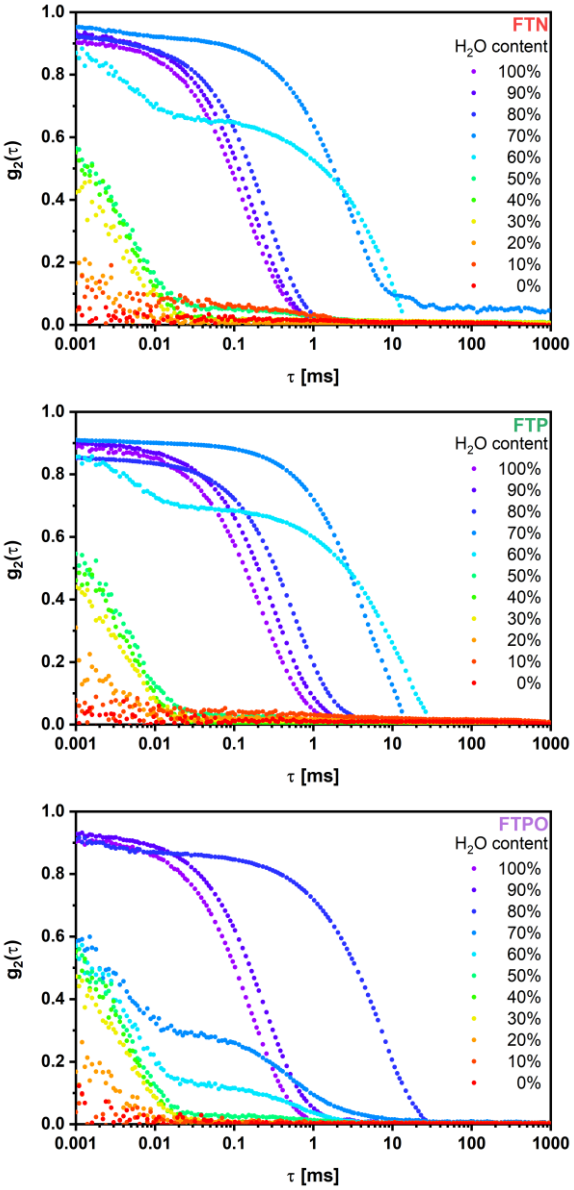

Figure 7: Intensity auto-correlation functions $g_2(\tau)$ for **FTN**, **FTP**, and **FTPO** in THF/H_2O mixtures.

hand, aggregation induced by the anti-solvent. The former phenomenon is responsible for the changes at water fractions of up to 60 vol%. When we compare the fluorescence spectra obtained at 70 vol% and more to the spectra from powder samples, we note a significant similarity. Therefore, we infer that the same intermolecular excited state interactions are present in the aggregates as in the solid state. These findings can be rationalized by the observation that interactions between two **F** molecules quench the fluorescence (see the SI, section 7.7.1, for TDDFT calculations in vacuum), which is known from the literature.[21] In aggregates of **FTP** and **FTPO,** in which numerous fluorene–fluorene contacts are present, fluorescence from the fluorenes is suppressed similarly to previous experimental findings for polymers comprising fluorene moieties.[54]

Information about the nature of the aggregates in the dispersions was gathered by means of dynamic and static light scattering (DLS and SLS). We recorded the static scattering intensity of the samples, a measure for the number and size of particles, as a function of the water content (Figure 6, black dots). Below 60 vol%, no noteworthy scattering is observed for **FTN**. As the fraction of water reaches 60 vol%, the sample becomes opaque and significant scattering is detected. For **FTN**, this finding verifies the formation of particles and marks the crossing of the binodal point.[28] Initially, the intensity increases with the water content as supersaturation is reached, and more and/or larger particles are formed. As the fraction of water surpasses 70 vol%, the scattering intensity starts to decline. The combination of negligible solubility and high grade of supersaturation generates vast amounts of particles at high water contents. Eventually, coalescence, creaming, and precipitation reduce the number of particles. We note similar trends in the case of **FTP**, for which the sample with 70 vol% H_2O exhibits the strongest scattering intensity. In contrast, **FTPO** is better soluble in the THF/H_2O mixtures, and significant particle formation starts at 70 vol% H_2O, whereby a steady increase of the intensity with increasing water content is noted.

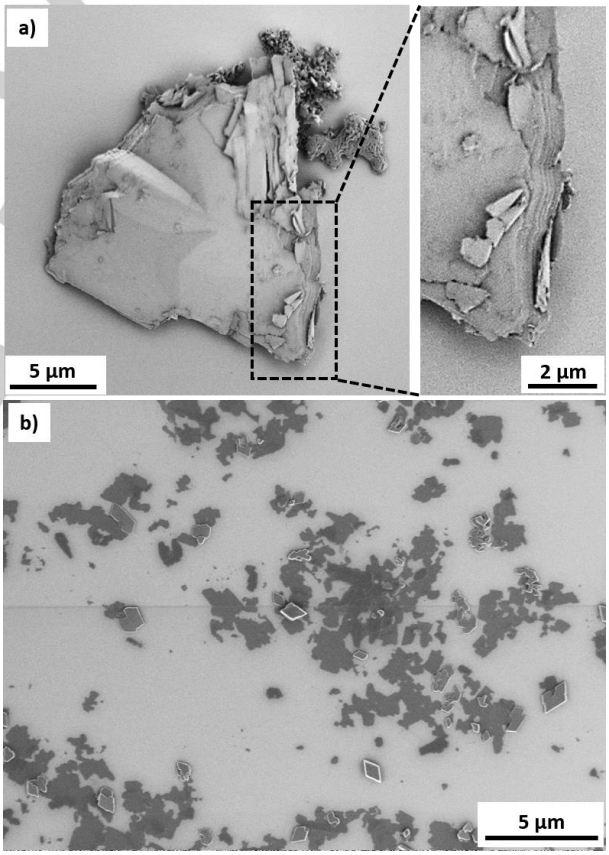

Figure 8: Representative SEM micrographs of (a) a large-sized crystal with layered structure as well as (b) ultrathin nanosheets and small-sized crystallites (b) of **FTN** from a THF/H_2O= 50/50 (v/v) dispersion.

Complementary, in DLS, we obtained the relaxation times from the electric field autocorrelation functions (Figure 7) and calculated the hydrodynamic radii of the particles (Figure 6, red dots). The radii for **FTN** start at a size of above R_H = 2.3 µm and reduce to an R_H = 60 nm by increasing the ratio of water in the solution. The sizes of the particles follow a similar trend starting with high R_H values at R_H = 4.7 µm, which decreases to R_H = 137 nm with the rising water content in the solvent mixture. In the case of **FTPO**, particle formation sets in at 70 vol% and a size of R_H = 474 nm. From there, it rises up to R_H = 1.37 µm and decreases from there to R_H = 117 nm. In general, the particle size

decreases as the amount of water is increased. At lower water content, nucleation dominates and, in turn, particle growth sets in with the supersaturated solvent continuum as feedstock. In contrast, at higher water content nucleation occurs in multiple locations, and particle growth is suppressed.

To gain more detailed information about the impact of the solvent mixture on the morphology of the aggregates formed from **FTN**, **FTP**, and **FTPO**, scanning electron microscopy (SEM) studies were carried out. To this end, the aggregates obtained from the three representative THF/H_2O mixtures containing 50, 70, and 90 vol% H_2O were investigated. For all samples, the concentrations were set to 2×10^{-6} M, which is the same as used in the fluorescence and dynamic light scattering aggregation studies. The aggregates were collected by drop-casting of the dispersion on silicon wafer. The rest liquid of the droplet was drawn off after 40 sec. to avoid the formation of excessive aggregates during the drying process.

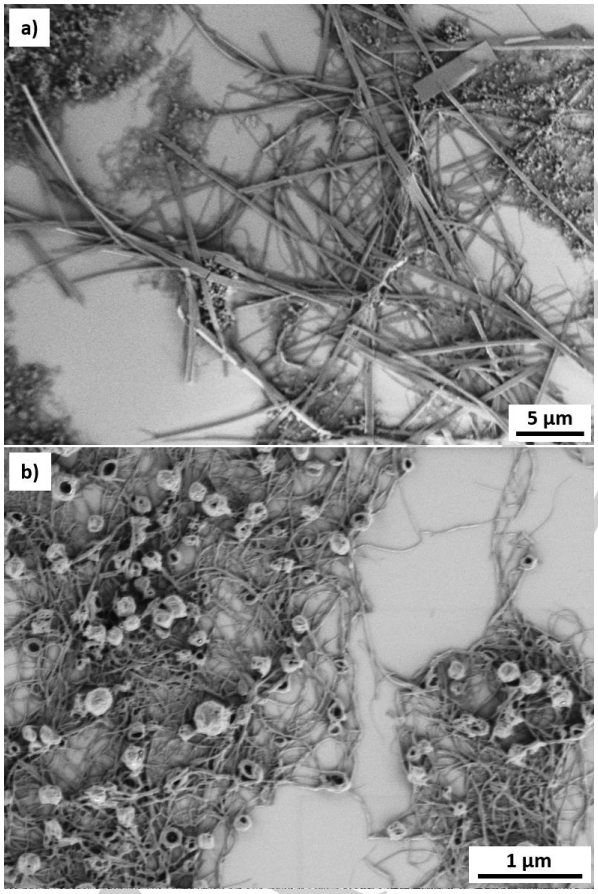

Figure 9: SEM micrographs of **FTPO** from a THF/H_2O = 30/70 (v/v) dispersion: formation of (a) needles and (b) nanofibers and hollow spheres weaved therefrom.

A first morphological overview is obtained by using optical microscopy (see the SI, Figure S46). Large microcrystals with a diameter of up to 50 µm as well as small particles in the range from a few µm to sub-µm are observed in all samples. SEM investigations revealed more morphological details: Large microcrystals appear as stacks of two-dimensional layers. As exemplified in Figure 8a, (**FTN** in the 50 vol% H_2O mixture, other cases see Figure S47), the 2D layers are loosely compressed and are partly exfoliated via simple mechanical forces, such as shaking or stirring, suggesting weak interlayer interactions. Next to stacks, µm-sized single nano-sheets are also found in 50 vol% H_2O mixtures of **FTN**, **FTP** and **FTPO** (see Figure 8b, Figure S50 and Figure S53) as well as in 70 vol% H_2O mixtures of **FTN** and **FTP** (see Figure S48 and Figure S51). One-dimensional needles with length of several tens of µm appear in both the 70 vol% H_2O mixtures of **FTP** and **FTPO** (see Figure S51 and Figure 9a). Distinguished from the other two heterotriangulenes, **FTPO** forms predominantly one-dimensional structures in the 70 vol% H_2O mixtures. Besides needles, the dispersion contains also a large number of 20-30 nm wide crystalline nano-fibers, weaving occasionally hollow spheres and halfspheres with diameters of 50-100 nm. Such a tendency of **FTPO** to form nano-fibers is already found in H_2O content lower than 50 vol% (see Figure S53). In the 90 vol% H_2O mixtures of **FTN**, **FTP** and **FTPO** (see Figure S49, Figure S52 and Figure S55), low-dimensional crystalline aggregates are noted in only a few cases. Instead, amorphous aggregates, like spheres and irregularly shaped particles, are predominately formed; crystal growth is suppressed due to the high content of anti-solvent. In general, **FTN**, **FTP** and **FTPO** show a strong crystallization tendency in the H_2O/THF mixtures and favor low dimensional crystalline aggregates with multiple morphologies. Fine-tuning of the crystallization conditions may rise the possibility to obtain aggregates in single morphology with a desired size distribution.

Conclusion

In summary, we complemented the series of a previously reported spirofluorene-bridged triphenylamine **FTN** and phosphine oxide **FTPO** with the structurally related triphenylphosphine **FTP**. Our work provides valuable insights into the impact, which evolves from a small structural adjustment, namely the variation of the central heteroatom on fluorescence, charge distribution, and pyramidalization relative to macroscopic properties such as aggregation and morphology.

Upon aggregation the dual fluorescent features of **FTN**, **FTP**, and **FTPO** converged to those obtained from the solid state, with core emission that evolves at the expense of the fluorene centered fluorescence. It was assumed that the intermolecular interactions in the excited state within aggregates are, therefore, similar to those in the solid state. They are dominated by dispersive interactions ($C(sp^2)$–H···π and π···π). For **FTP**, dispersive interactions are even stronger than the dipole-dipole interactions. In turn, dimers with opposing dipole moments are formed as substructures. This unexpected turnover, illustrates the unpredictability of solid state interactions, even within a series of structurally similar molecules. The aggregate morphology showed high crystallinity at 70 vol% H_2O and turned into amorphous structures at 90 vol% H_2O.

The perpendicularly oriented π-systems, which we present in this work, constitute a versatile platform for further functionalization. By virtue of weak electronic interactions between the components we anticipate that the individual subunits, that is, the heterotriangulene core and the fluorenyl wings, shall be readily adjustable to create functional materials. In general, spiro-compounds have found tremendous interest, and spiro-OMeTAD,[55-57] a prominent hole transport material, is probably one of the best known example. In particular, structurally related triarylamines and the corresponding phosphines (and their

oxides) have already been employed as charge transport materials in organic photovoltaic cells and light emitting devices[56-59] or host matrices in light emitting diodes.[58,60-63] Motivated by such a unique perspective we are currently developing materials derived from the spiro-heterotriangulene skeleton presented in this work for device application.

Acknowledgements

The generous funding by the Deutsche Forschungsgemeinschaft (DFG) – Project number 182849149 – SFB 953 and project number 401247651 – KI 1662/3-1 is acknowledged. M. B. thanks the support from the projects ANR PRC WSPLIT (ANR-17-CE05-0005-01) and Equip@Meso (ANR-10-EQPX-29-01). W.-S. Z. and R. R. S. acknowledge funding by the Deutsche Forschungsgemeinschaft, SFB 1249.

Keywords: spiro compounds • heteropolycycles • aggregation • photophysics • morphology • density functional theory (DFT) calculations

[1] F. Würthner, C. R. Saha-Möller, B. Fimmel, S. Ogi, P. Leowanawat, D. Schmidt, *Chem. Rev.* **2016**, *116*, 962–1052.
[2] L. Maggini, D. Bonifazi, *Chem. Soc. Rev.* **2012**, *41*, 211–241.
[3] E. Gomar-Nadal, J. Puigmartí-Luis, D. B. Amabilino, *Chem. Soc. Rev.* **2008**, *37*, 490–504.
[4] S. Ghosh, D. S. Philips, A. Saeki, A. Ajayaghosh, *Adv. Mater.* **2017**, *29,* 1605408.
[5] R. Pfukwa, P. H. J. Kouwer, A. E. Rowan, B. Klumperman, *Angew. Chem. Int. Ed.* **2013**, *52*, 11040–11044; *Angew. Chem*. **2013**,*125*, 11246 –11250.
[6] A. Malliaris, J. Le Moigne, J. Sturm, R. Zana, *J. Phys. Chem.* **1985**, *89*, 2709–2713.
[7] D. W. Cho, D. W. Cho, *New J. Chem.* **2014**, *38*, 2233–2236.
[8] J. Puigmartí-Luis, Á. Pérez Del Pino, V. Laukhin, L. N. Feldborg, C. Rovira, E. Laukhina, D. B. Amabilino, *J. Mater. Chem.* **2010**, *20*, 466–474.
[9] M. Son, K. H. Park, C. Shao, F. Würthner, D. Kim, *J. Phys. Chem. Lett.* **2014**, *5*, 3601–3607.
[10] K. Dirian, S. Bauroth, A. Roth, Z. Syrgiannis, F. Rigodanza, M. Burian, H. Amenitsch, D. I. Sharapa, M. Prato, T. Clark, D. M. Guldi, *Nanoscale* **2018**, *10*, 2317–2326.
[11] S. Schöttl, D. Horinek, *Curr. Opin. Colloid Interface Sci.* **2016**, *22*, 8–13.
[12] A. Modaressi, H. Sifaoui, M. Mielcarz, U. Domańska, M. Rogalski, *Colloids Surfaces A Physicochem. Eng. Asp.* **2007**, *302*, 181–185.
[13] H. Chen, M. S. Farahat, K. Y. Law, D. G. Whitten, *J. Am. Chem. Soc.* **1996**, *118*, 2584–2594.
[14] T. Ishi-I, K. Ikeda, M. Ogawa, Y. Kusakaki, *RSC Adv.* **2015**, *5*, 89171–89187.
[15] T. Miletić, A. Fermi, I. Orfanos, A. Avramopoulos, F. De Leo, N. Demitri, G. Bergamini, P. Ceroni, M. G. Papadopoulos, S. Couris, D. Bonifazi, *Chem. Eur. J.* **2017**, *23*, 2363–2378.
[16] M. Kasha, H. R. Rawls, M. Ashraf El-Bayoumi, *Pure Appl. Chem.* **1965**, *11*, 371–392.
[17] M. Kasha, *Radiat. Res.* **1963**, *20*, 55.
[18] J. L. Bricks, Y. L. Slominskii, I. D. Panas, A. P. Demchenko, *Methods Appl. Fluoresc.* **2018**, *6*, 012001.
[19] N. J. Hestand, F. C. Spano, *Acc. Chem. Res.* **2017**, *50*, 341–350.
[20] F. Würthner, T. E. Kaiser, C. R. Saha-Möller, *Angew. Chem. Int. Ed.* **2011**, *50*, 3376–3410; *Angew. Chem.* **2011**,*123*, 3436–3473.
[21] J. P. Pinion, F. L. Minn, N. Filipescu, *J. Lumin.* **1971**, *3*, 245–252.
[22] J. E. Wittmann, L. M. S. Stiegler, C. Henkel, J. Träg, K. Götz, T. Unruh, D. Zahn, A. Hirsch, D. Guldi, M. Halik, *Adv. Mater. Interfaces* **2019**, *6*, 1801930.
[23] M. Wolffs, F. J. M. Hoeben, E. H. A. Beckers, A. P. H. J. Schenning, E. W. Meijer, *J. Am. Chem. Soc.* **2005**, *127*, 13484–13485.
[24] E. R. Sauvé, C. M. Tonge, Z. M. Hudson, *J. Am. Chem. Soc.* **2019**, *141*, 16422–16431.
[25] A. de la Escosura, M. V. Martínez-Díaz, P. Thordarson, A. E. Rowan, R. J. M. Nolte, T. Torres, *J. Am. Chem. Soc.* **2003**, *125*, 12300–12308.
[26] M. Koenig, T. Torres, V. Barone, G. Brancato, D. M. Guldi, G. Bottari, *Chem. Commun.* **2014**, *50*, 12955–12958.
[27] T. A. Schaub, S. M. Brülls, P. O. Dral, F. Hampel, H. Maid, M. Kivala, *Chem. Eur. J.* **2017**, *23*, 6988–6992.
[28] E. Middha, P. N. Manghnani, D. Z. L. Ng, H. Chen, S. A. Khan, B. Liu, *Mater. Chem. Front.* **2019**, *3*, 1375–1384.
[29] M. M. Xiu, Q. Kang, M. L. Tao, Y. Chen, Y. Wang, *J. Mater. Chem. C* **2018**, *6*, 5926–5936.
[30] T. A. Schaub, T. Mekelburg, P. O. Dral, M. Miehlich, F. Hampel, K. Meyer, M. Kivala, *Chem. Eur. J.* **2020**, *26*, 3264–3269.
[31] T. A. Schaub, E. M. Zolnhofer, D. P. Halter, T. E. Shubina, F. Hampel, K. Meyer, M. Kivala, *Angew. Chem. Int. Ed.* **2016**, *55*, 13597–13601; *Angew. Chem.* **2016**,*128*,13795–13799.
[32] T. Imamoto, S.-i. Kikuchi, T. Miura, Y. Wada, *Org. Lett.* **2001**, *3*, 87–90.
[33] T. Coumbe, N. J. Lawrence, F. Muhammad, *Tetrahedron Lett.* **1994**, *35*, 625–628.
[34] M. Berthod, C. Saluzzo, G. Mignani, M. Lemaire, *Tetrahedron Asymmetry* **2004**, *15*, 639–645.
[35] T. A. Modro, *Can. J. Chem.* **1977**, *55*, 3681–3685.
[36] A. E. Reed, P. von Ragué Schleyer, *J. Am. Chem. Soc.* **1990**, *112*, 1434–1445.
[37] T. Leyssens, D. Peeters, *J. Org. Chem.* **2008**, *73*, 2725–2730.
[38] T. Baumgartner, *Acc. Chem. Res.* **2014**, *47*, 1613–1622.
[39] J. Da Chai, M. Head-Gordon, *Phys. Chem. Chem. Phys.* **2008**, *10*, 6615–6620.
[40] F. Weigend, R. Ahlrichs, *Phys. Chem. Chem. Phys.* **2005**, *7*, 3297–3305.
[41] T. A. Schaub, R. Sure, F. Hampel, S. Grimme, M. Kivala, *Chem. Eur. J.* **2017**, *23*, 5687–5691.
[42] A. D. Becke, *J. Chem. Phys.* **1993**, *98*, 5648–5652.
[43] P. J. Stephens, F. J. Devlin, C. F. Chabalowski, M. J. Frisch, *J. Phys. Chem.* **1994**, *98*, 11623–11627.
[44] S. Grimme, P. R. Schreiner, *Angew. Chem. Int. Ed.* **2011**, *50*, 12639–12642; *Angew. Chem.* **2011**,*123*, 12849–12853.
[45] D. Hellwinkel, M. Melan, *Chem. Ber.* **1974**, *107*, 616–626.
[46] D. Hellwinkel, A. Weil, G. Sattler, B. Nuber, *Angew. Chem. Int. Ed.* **1990**, *29*, 689–692; *Angew. Chem.* **1990**, *102*, 677–680.
[47] F. Plasser, M. Wormit, A. Dreuw, *J. Chem. Phys.* **2014**, *141*, 024106.
[48] H. Dürr, R. Gleiter, *Angew. Chem. Int. Ed.* **1978**, *17*, 559–569; *Angew. Chem.* **1978**, *90*, 591–601.
[49] A. Schweig, U. Weidner, J. G. Berger, W. Grahn, *Tetrahedron Lett.* **1973**, *14*, 557–560.
[50] A. Schweig, U. Weidner, D. Hellwinkel, W. Krapp, *Angew. Chem. Int. Ed.* **1973**, *12*, 310–311; *Angew. Chem.* **1963**, *85*, 360–361.
[51] D. L. Horrocks, W. G. Brown, *Chem. Phys. Lett.* **1970**, *5*, 117–119.
[52] H. K. Kang, D. E. Kang, B. H. Boo, S. J. Yoo, J. K. Lee, E. C. Lim, *J. Phys. Chem. A* **2005**, *109*, 6799–6804.
[53] Y. B. Chung, D.-J. Jang, D. Kim, M. Lee, H. S. Kim, B. H. Boo, *Chem. Phys. Lett.* **1991**, *176*, 453–458.
[54] J. Shi, Y. Wu, S. Sun, B. Tong, J. Zhi, Y. Dong, *J. Polym. Sci. Part A Polym. Chem.* **2013**, *51*, 229–240.
[55] U. Bach, D. Lupo, P. Comte, J. E. Moser, F. Weissörtel, J. Salbeck, H. Spreitzer, M. Grätzel, *Nature* **1998**, *395*, 583–585.
[56] S. Gangala, R. Misra, *J. Mater. Chem. A* **2018**, *6*, 18750–18765.
[57] C. H. Teh, R. Daik, E. L. Lim, C. C. Yap, M. A. Ibrahim, N. A. Ludin, K. Sopian, M. A. Mat Teridi, *J. Mater. Chem. A* **2016**, *4*, 15788–15822.
[58] D. Joly, P.-A. Bouit, M. Hissler, *J. Mater. Chem. C* **2016**, *4*, 3686–3698.
[59] J. Wang, K. Liu, L. Ma, X. Zhan, *Chem. Rev.* **2016**, *116*, 14675–14725.
[60] T. Liu, H. Sun, C. Fan, D. Ma, C. Zhong, C. Yang, *Org. Electron.* **2014**, *15*, 3568–3576.
[61] S. O. Jeon, K. S. Yook, C. W. Joo, J. Y. Lee, *J. Mater. Chem.* **2009**, *19*, 5940–5944.
[62] X. Cai, A. B. Padmaperuma, L. S. Sapochak, P. A. Vecchi, P. E. Burrows, *Appl. Phys. Lett.* **2008**, *92*, 90–93.
[63] S. O. Jeon, K. S. Yook, C. W. Joo, J. Y. Lee, *Adv. Mater.* **2010**, *22*, 1872–1876.

10.1002/anie.202003504

WILEY-VCH

RESEARCH ARTICLE

Entry for the Table of Contents

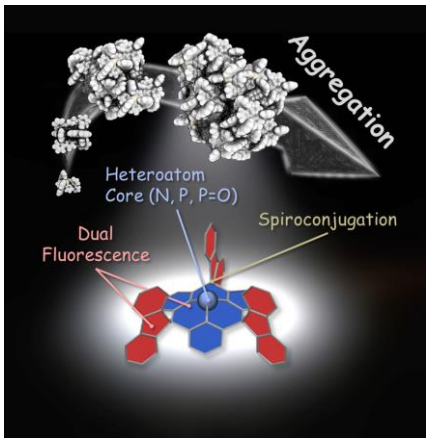

Make a difference together. Heteroatoms were inserted into spiro-conjugated triangulenes and the resultant structure-property relationships were explored. At the focal point are the molecular and electronic structure, their dual fluorescence (core and wings), and their aggregation behavior in solvent anti-solvent mixtures.

Institute and/or researcher Twitter usernames: @GroupGuldi